JOURNAL OF GEOPHYSICAL RESEARCH, VOL. 103, NO. B12, PAGES 30,269–30,282, DECEMBER 10, 1998

Late Neogene exhumation patterns in Taranaki Basin (New Zealand): Evidence from offset porosity-depth trends

Phillip A. Armstrong

Department of Geology and Geophysics, University of Utah, Salt Lake City

Richard G. Allis[1] and Robert H. Funnell

Institute of Geological and Nuclear Sciences, Lower Hutt, New Zealand

David S. Chapman

Department of Geology and Geophysics, University of Utah, Salt Lake City

Abstract. Taranaki Basin, New Zealand, is located adjacent to the Australian-Pacific Plate boundary where the tectonic regime changes from dominantly subduction-related to the north to transpression-related along the Alpine Fault to the south. During the Neogene, burial and exhumation varied extensively, in both time and space, in response to subsidence and uplift along this evolving plate boundary zone. The basin can be divided into two regions: (1) the Western Platform outside the plate boundary deformation zone where no uplift nor exhumation has occurred and (2) the Eastern Mobile Belt, which lies inside the deformation zone and has been variably uplifted and exhumed. Exhumation magnitudes for sedimentary deposits of the basin are estimated from offset porosity-depth trends. The analysis is based on correlating sonic log travel times with compensated density logs, permitting sonic travel time to be used as a proxy for porosity. Twelve Western Platform wells are used to define a standard exponential porosity-depth trend with an extrapolated surface porosity of 50% and an exponential decay factor of 2265 m, valid for mudstone/shale sections spanning a depth range of 300-3000 m. This curve is a calibration curve against which offset porosity-depth trends from wells in exhumed regions can be compared to determine apparent exhumation amounts. Porosity-depth trends for 43 Eastern Mobile Belt wells are offset 0-2800 m shallower relative to the Western Platform trend but generally are parallel to it. In the southern region of the Eastern Mobile Belt, net exhumation amounts, which are the sum of the porosity-depth trend offset and depth to unconformity, range from 850 to 3000 m; most of this exhumation occurred on discrete contractional structures in late Miocene to early Pliocene time, probably associated with an increased rate of convergence across the Alpine Fault system to the south. In the eastern region of the Eastern Mobile Belt, net exhumation progressively increases from 0 m in the south to 1800 m in the northeast part of the basin, consistent with the 2°-4° SW structural tilt of onshore strata. The regional and consistent pattern of exhumation in the eastern region contrasts with the discrete structure-related exhumation in the southern region and is consistent with models of thermal and flexural uplift.

1. Introduction

Taranaki Basin is located partially in the deformation zone associated with the Australian-Pacific Plate boundary (Figure 1) where the tectonic regime changes from a dominantly subduction-related back arc and magmatic arc setting to the north to a transpressive setting related to movement along the Alpine Fault to the south. The stratigraphic record of the basin, which has been extensively explored for hydrocarbons, contains a rich record of its complex Neogene tectonic history. In particular, the basin deposits contain information about past uplift and exhumation events that occurred in response to the evolving plate interactions. Estimates of past exhumation variations, in both space and time, should provide valuable constraints for geodynamic modeling of this area.

Several methods have been used to estimate exhumation amounts in Taranaki and elsewhere. Probably the most common method in basin studies employs seismic reflection sections [e.g., *Knox*, 1982; *Ellyard and Beattie*, 1990]. Exhumation amounts are estimated on the basis of amounts of missing section across faults or over folds, but these estimates require knowledge or assumptions about the initial thickness of eroded material. Also, unconformities with no angular discordance are common, making them difficult to interpret on the basis of seismic data. Proxy indicators of past burial amounts, such as vitrinite reflectance [*Sykes et al.*, 1992] and fission track [*Kamp and Green*, 1990] data, can provide very

[1]Now at Energy and Geoscience Institute, University of Utah Research Park, Salt Lake City.

Paper number 98JB02843.
0148-0227/98/98JB-02843$09.00

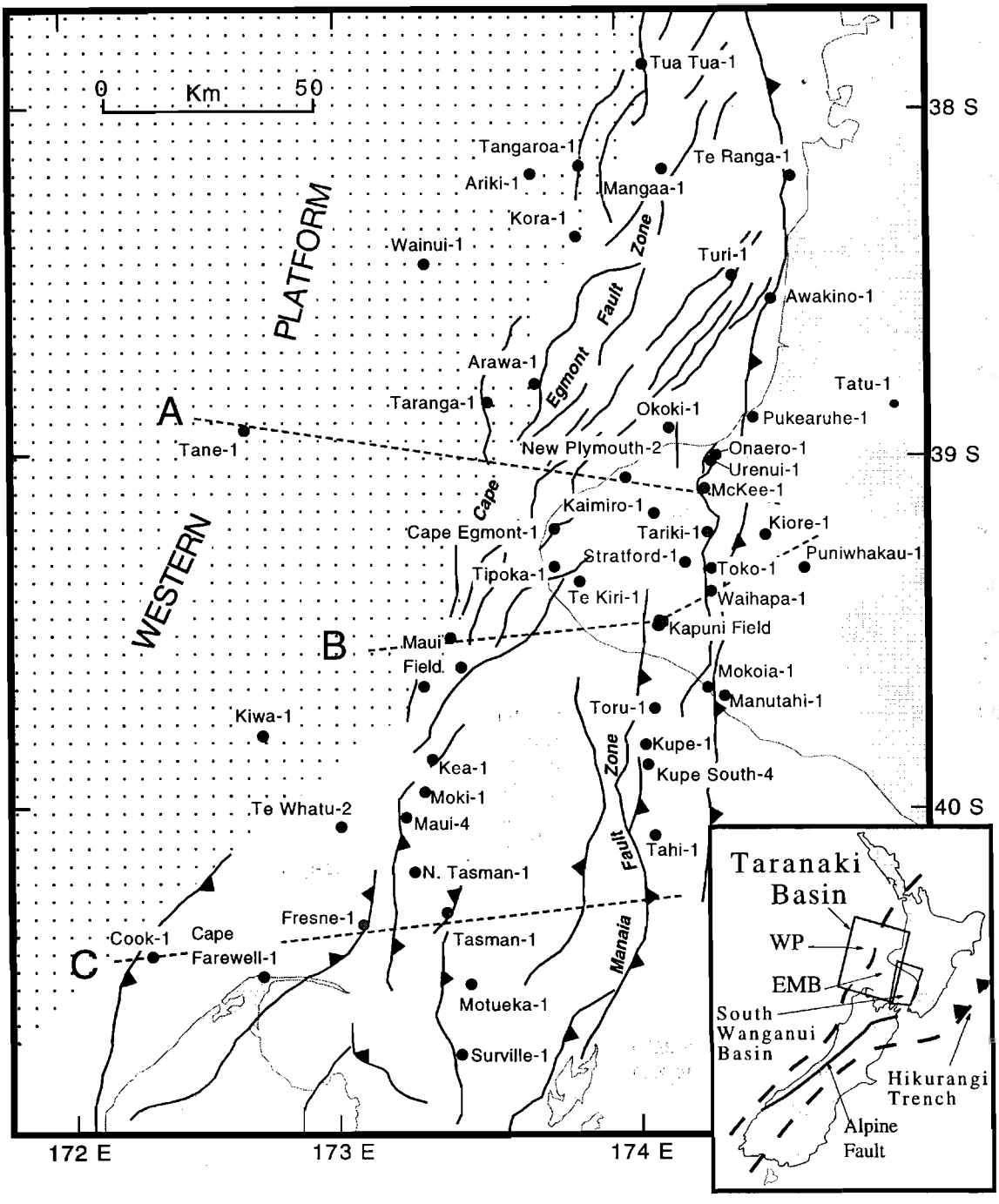

Figure 1. Location map showing wells used in this study and major faults. Stippled area is Western Platform. Area to east and southeast of Western Platform is the Eastern Mobile Belt. Inset map shows position of Taranaki Basin relative to plate boundary zone (outlined by bold dashes). WP is Western Platform; EMB is Eastern Mobile Belt. Maui Field contains all the Maui wells except Maui-4, and Kapuni Field contains all the Kapuni wells used in this study.

good estimates of exhumation. However, use of these thermal indicators depends on assumptions regarding paleogeothermal gradients. Uplifted terraces and other geomorphic features also give estimates of recent (Quaternary) uplift [*Pillans*, 1986]. Over longer periods of time, erosion must be taken into account to deduce absolute uplift of the surface [*England and Molnar*, 1990].

The method of estimating exhumation applied in this paper is based on porosity-depth variations as first described by *Magara* [1976]. Standard porosity-depth profiles for areas thought to represent noneroded sections of rock that are presently at maximum burial depths are compared to porosity-depth profiles from disturbed (exhumed) sections to give estimates of exhumation. This method has been used in several regions including the Western Canada Basin [*Magara*, 1976], the Beaufort-Mackenzie Basin [*Issler*, 1992], the Bighorn Basin [*Heasler and Kharitonova*, 1996], and the North Island of New Zealand [*Wells*, 1990].

In this paper we utilize offset porosity-depth trends to evaluate exhumation amounts and patterns in the Taranaki Basin, New Zealand (Figure 1). Taranaki Basin is ideal for this type of analysis because (1) it has a region (Western Platform; Figure 1) that is at maximum burial where no known erosion has occurred and from which well-constrained standard porosity-depth profiles can be extracted, (2) it consists of a dominantly silty mudstone lithology that provides thick portions of the sedimentary section whose porosity-depth profiles can be compared to the standard curves, and (3) it is composed of relatively young (Tertiary) sediments that are minimally affected by diagenetic effects that alter porosity and cause problems in porosity studies of older (Mesozoic and Paleozoic) strata.

2. Geologic Setting and Stratigraphy of the Taranaki Basin

Taranaki Basin is an active-margin basin that lies 400 km west of the Hikurangi Trench and 200 km above the subducting Pacific Plate on the western margin of the North Island of New Zealand (Figure 1). The structural, tectonic, and stratigraphic history of the region since the Late Cretaceous has been described extensively [e.g., *Pilaar and Wakefield*, 1978; *Knox*, 1982; *King and Thrasher*, 1992; *Holt and Stern*, 1994]; we briefly review the relevant Neogene geologic history below.

An important aspect of Taranaki Basin is that it can be divided into two principal regions, separated by the Cape Egmont Fault zone (Figure 1), that have distinctly different Neogene tectonic histories. The Western Platform region (Figure 1) has been relatively quiescent since the late Paleocene. The Eastern Mobile Belt has been variably affected by plate boundary deformation that caused significant and variable erosion amounts in the area.

In the early Neogene (25-35 Ma), development of the convergent plate boundary to the east caused basin-wide rapid subsidence of up to 2 km [*Hayward and Wood*, 1989]. In the earliest Miocene, contraction caused westward overthrusting in the eastern part of the basin. About 10 Ma the locus of contraction shifted from the northern and eastern parts of the basin to the southern and southeastern parts (Southern Inversion Zone of *King* [1994]), possibly causing extensive erosion and exhumation. During Plio-Pleistocene times, with the exception of the areas to the far south, the Taranaki Basin generally experienced extension, possibly related to backarc rifting. The Cape Egmont Fault Zone, a normal fault system that is active today, formed along reactivated reverse faults. Late Pleistocene southwest tilting (2°-4°) centered on the south part of the South Wanganui Basin (Figure 1) affected the Taranaki Peninsula and adjacent offshore region to the south. Late Quaternary uplift of beach and river terraces indicates that rates of uplift on the Taranaki Peninsula have been ~0.25 mm yr^{-1} for the last 100,000 years [*Pillans*, 1986]. The Western Platform region has been relatively quiescent with only monotonic subsidence.

Thick sequences of silty mudstone were deposited during the Miocene. In Plio-Pleistocene times, uplift and exhumation of the Southern Alps to the south provided abundant terrigenous material that was deposited as sandstone and mudstone in the east and dominantly mudstone and siltstone of the Giant Foresets Formation in the Western Platform region. Plio-Pleistocene deposits are relatively thick across much of the basin, locally reaching thicknesses of up to 3000 m [*Thrasher and Cahill*, 1990].

Maximum sediment thicknesses range from ~4 km on the Western Platform and in the South Wanganui Basin to the east to ~8 km locally in the Eastern Mobile Belt (Figure 2). Known unconformities occur at the top of the Miocene in southern wells of the Eastern Mobile Belt and at the surface or just below the Quaternary volcanic deposits in onshore wells of the Eastern Mobile Belt. It is important to note that no unconformities are located in the Western Platform wells, thus providing an uninterrupted sequence of dominantly Tertiary fine-grained terrigenous strata.

3. Porosity Evaluation

Porosity generally decreases with increasing depth in sedimentary rocks under hydrostatic load [*Gallagher*, 1989; *Heasler and Kharitonova*, 1996]. The most commonly used porosity-depth relation is an exponential function

$$\phi(z) = \phi_o \exp(-z/D) \quad (1)$$

originally proposed by *Athy* [1930] and later suggested by many others [e.g., *Magara*, 1976; *Sclater and Christie*, 1980; *Korvin*, 1984]. Surface porosity is ϕ_o, z is depth, and D is an exponential decay constant. Other porosity-depth functions have been proposed for shales [*Magara*, 1978; *Selley*, 1978; *Falvey and Deighton*, 1982; *Korvin*, 1984; *Baldwin and Butler*, 1985; *Wells*, 1990; *Issler*, 1992], but they have a form similar to (1).

Like porosity, travel time (the inverse of compressional velocity recorded on sonic logs) generally decreases as a function of decreasing porosity and increasing depth. Empirical fits to travel time data as a function of depth have been described as exponential [*Magara*, 1976; *Heasler and Kharitonova*, 1996]. In Taranaki Basin, travel times vary markedly at all depths but display less variability at deeper depths (Figure 3a). These data are from three different regions of the basin: Western Platform, east Taranaki, and south Taranaki. The Western Platform region has been relatively undisturbed, whereas the eastern and southern regions contain unconformities on which variable amounts of exhumation have occurred (Figure 2). We correlated travel times with porosities determined from compensated formation density (FDC) logs (Figure 3b). Porosity is determined from the equation

$$\phi = (\rho_{ma} - \rho_{rock})/(\rho_{ma} - \rho_f) \quad (2)$$

where ρ_{ma} is matrix density, ρ_{rock} is density determined from the FDC logs, and ρ_f is density of the pore fluid. The matrix density is assumed to be 2700 kg m^{-3} on the basis of core measurements, and fluid density is assumed to be 1000 kg m^{-3}. Using different values of ρ_{ma} (2650-2750 kg m^{-3}) results in ~7% relative variation in porosity values at typical rock absolute porosities of 30% (±2% absolute porosity units). Travel time (tt) at each FDC measurement depth was integrated over a 100 m depth interval. Generally, the Taranaki density versus travel time values plot between the empirical curves of *Issler* [1992] for shale and *Wyllie et al.* [1956] for sandstone (Figure 3b). There is considerable scatter in the data, probably reflecting variations in silt content of the Taranaki mudstones. The best fit third-order polynomial ($R = 0.95$) is

$$\phi(tt) = -74.7 + 0.532(tt) - 9.8\times10^{-4}(tt^2) + 7.26\times10^{-7}(tt^3). \quad (3)$$

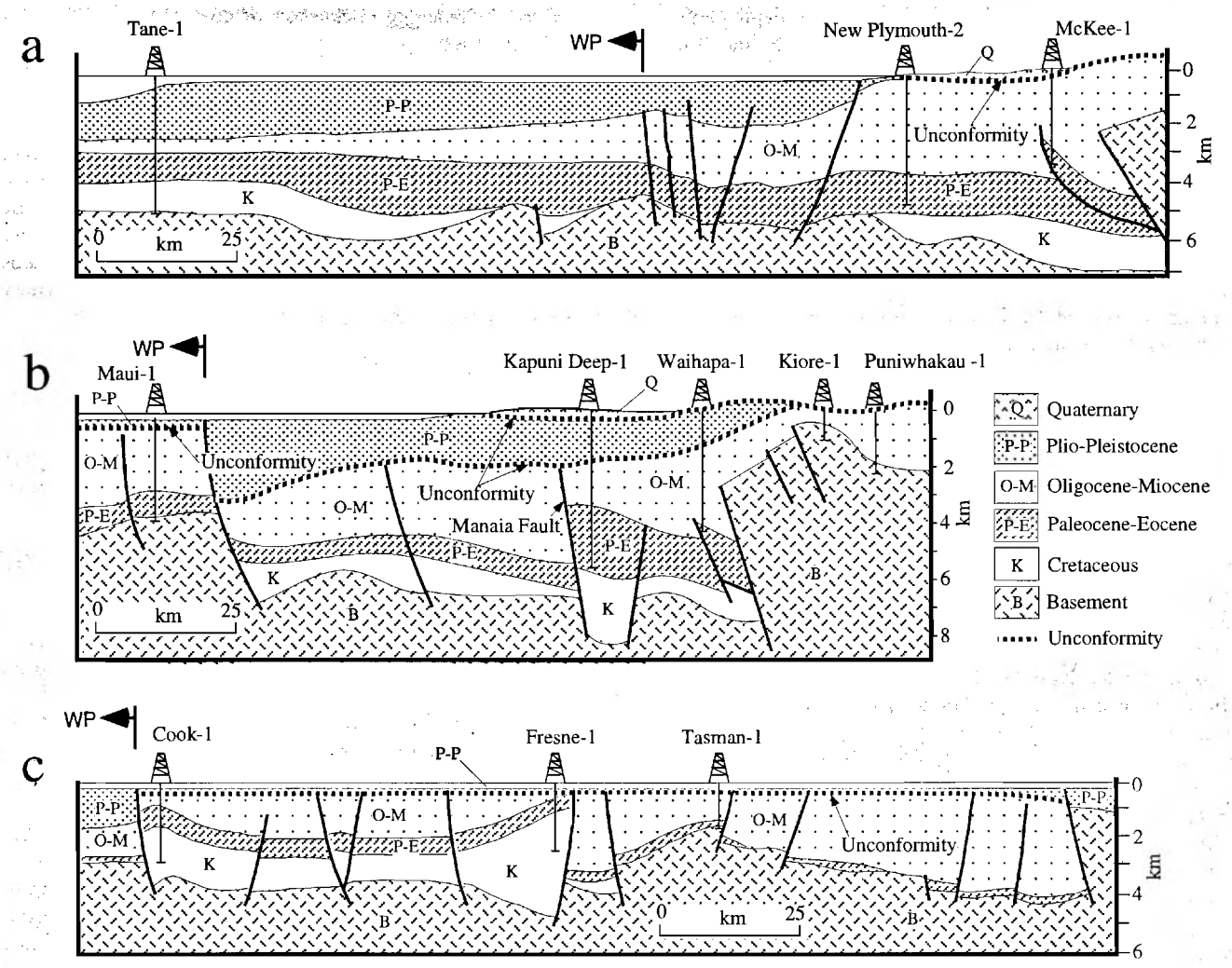

Figure 2. Representative cross sections across Taranaki Basin [after *King et al.*, 1991; *King and Thrasher*, 1996]. See Figure 1 for locations. WP is Western Platform.

The misfits of FDC porosity to the polynomial have a standard deviation of 3% absolute porosity. Equation (3) is similar to the density versus travel time curve of *Davis and Villinger* [1992] for a 50-50 mix of mudstone and sandstone from offshore western Canada (Figure 3b). We acknowledge that there is no physical basis for the third-order polynomial fit and that the absolute shape of the porosity-depth trend would change slightly if another porosity versus travel time relation (e.g., second-order polynomial) were used. However, the absolute porosity uncertainty (±3%) and relative changes between the standard and offset porosity-depth trends would not change.

3.1. Taranaki Standard Porosity-Depth Curve

FDC porosity for wells from the Western Platform region, with the exception of high-porosity data from depths of 2.8-3.4 km, decreases with depth (Figure 4a). The anomalously high porosity data are from a region of probable overpressure, which is common at these depths in the Taranaki Basin [*King and Thrasher*, 1996] and in many basins around the world. The best fit (R = -0.96) occurs with a surface porosity of 50% and a D value of 2265 m, thus leading to the standard porosity-depth curve for Taranaki mudstones:

$$\phi(z) = 50 \exp(-z/2265). \quad (4)$$

These results are based on data from the 11 Western Platform wells and one well located just within the Eastern Mobile Belt (Mangaa-1). We include well Mangaa-1 because it is in a region that displays no apparent unconformities even though it is east of the Cape Egmont Fault zone (Figure 1). Computed sonic porosities for the Western Platform show a good fit to the standard porosity-depth curve (Figure 4b), thus indicating that the transformation from sonic-derived travel times to porosity is well constrained.

The uncertainties in D and ϕ_0 of (4) correspond to ~±100 m and ±1% absolute porosity, respectively. However, these uncertainties give little information about how much regional variability in porosity versus depth there is from well site to well site where exhumation is known to be zero and where porosity may be partly controlled by variations in rock type, mineralogy, and diagenesis. The good fit of the data for each well to the average model curve (Figure 5) indicates that there is little variability in the porosity-depth trends at well sites across the ~200 km wide Western Platform region. "Bootstrapping" statistical experiments [e.g., *Press et al.*, 1992], whereby porosity data from each well on the Western Platform are compared to the data from the other 11 wells,

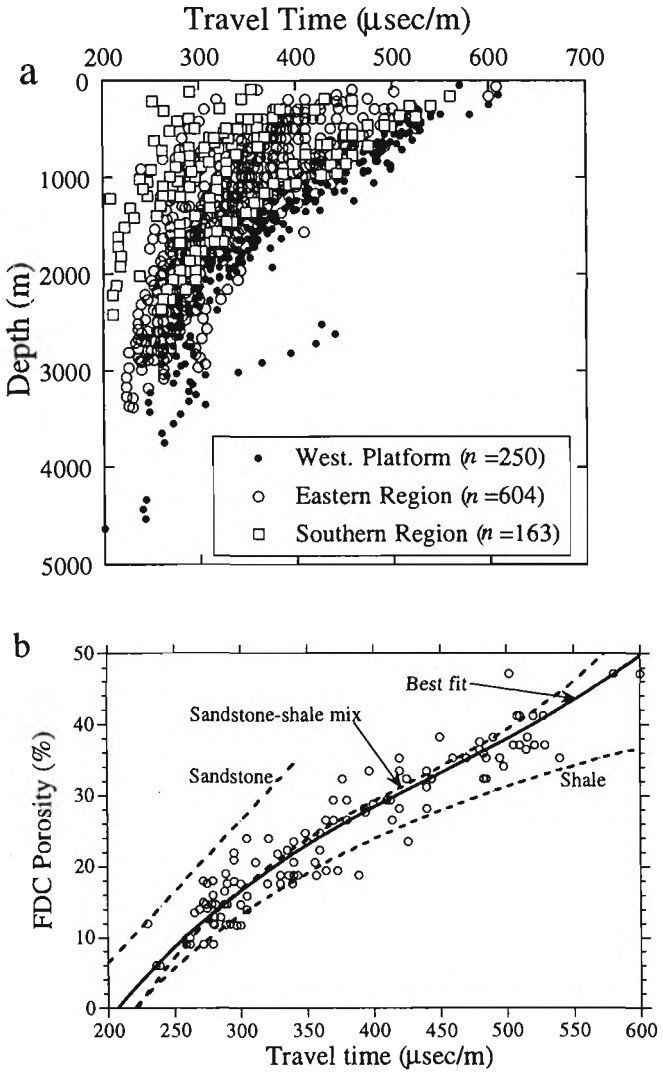

Figure 3. Travel time versus (a) depth and (b) compensated formation density-determined porosity (FDC) for Taranaki mudstone/shale. In Figure 3a, travel time is averaged from 100 m intervals of industry sonic logs. In Figure 3b, the solid curve is the best fit third-order polynomial (R = 0.95). The dashed curves are from other studies for sandstone [*Wyllie et al.*, 1956], shale [*Issler*, 1992], and sandstone/shale mix [*Davis and Villinger*, 1992]. The Taranaki curve is similar to the mixed curve of *Davis and Villinger* [1992] because of a silty component to the Taranaki mudstones.

show that the uncertainty in the depth given by the standard curve (Figure 4 and equation (4)) is ~150 m for undisturbed Western Platform wells.

3.2. Deviations From the Standard Porosity-Depth Curve

Comparison of the depth offset between porosity-depth trends in exhumed sections and those of the standard curve gives estimates of apparent exhumation. Three examples of porosity-depth trends from Eastern Mobile Belt wells show the variability of relative porosity-depth trend offset from the Western Platform standard curve (Figure 6a). The curves through each of the data sets are of the form

$$\phi(z') = \phi_o' \exp(-z'/D) \quad (5)$$

where z' is depth and ϕ_o' is the best fit surface porosity for the potentially eroded section, assuming D = 2265 m as in the Western Platform region. Note that these are not best fit curves for each data set but are model curves. We assume that compaction rebound is minimal during exhumation of deeper rocks; compaction rebound tests on deep-sea terrigenous sediments show that rebound is only a few absolute porosity percent units [*Hamilton*, 1976]. Taking the natural logs of (1) and (5) and setting them equal to each other gives

$$\Delta z' = z - z' = [\ln(\phi_o) - \ln(\phi_o')]/(1/D) \quad (6)$$

where $\Delta z'$ is the average depth offset of the eroded section from the standard, noneroded section.

Porosity-depth trend offsets were determined for 43 Eastern Mobile Belt wells (Table 1). The amount of mudstone-shale section used relative to the total amount of section penetrated by the well averages ~50%, but ranges between 20% and 90% (Table 1). When the depth of each porosity data point is corrected by the depth offset ($\Delta z'$) for the corresponding well, the data show good correlation with the standard porosity-depth curve (Figure 6b). The correlation of the corrected depths to the standard porosity-depth curve and the high correlation coefficients of the model curves for most of the Eastern Mobile Belt wells (Table 1) suggest that the exponential decay constant (D) of the standard curve is applicable to the mudstone-shale sections of the entire basin.

For the three examples shown in Figure 6a the depth offsets are 270 (Maui-2), 850 (Kaimiro-1), and 2800 m (Fresne-1). Well Fresne-1 has the largest depth offset of any of the wells in the Taranaki Basin (Table 1). The porosity-depth trend for Fresne-1 shows more scatter than the other wells shown in Figure 6a and has one of the lowest correlation coefficients (R = - 0.78; Table 1). The scatter in Fresne-1 porosity is probably due to a higher degree of lithologic heterogeneity compared to other wells and to the maximum burial amounts of >3500 m where kerogen breakdown and dissolution of carbonate material may have caused significant overpressures and secondary porosity. Also, the greater amount of overburden removed at this well site may have allowed greater fracture porosity to form, especially at shallower depths.

The uncertainties in mean porosity offset ($\Delta z'$) values for each well are a combination of the uncertainties in the model fits to the data for both the standard curve from the Western Platform wells and the offset porosity curves from wells in areas that have experienced erosion. Estimates of uncertainties were determined formally using the quotient rule for error propagation [e.g., *Mood et al.*, 1974, p. 180]. If (6) is treated as the ratio of two independent variables ($[\ln(\phi_o) - \ln(\phi_o')]$ and $1/D$), then the standard deviation (σ) of the $\Delta z'$ values is given by

$$\sigma[\Delta z'] = \Delta z' \sqrt{\frac{\sigma[\ln(\phi_0)]^2 + \sigma[\ln(\phi_0')]^2}{\left(\ln(\phi_0) - \ln(\phi_0')\right)^2} + \frac{\sigma(1/D)^2}{(1/D)^2}} \quad (7)$$

where ϕ_o is 50% from the standard porosity curve, D is 2265 m for all wells, and ϕ_o' is determined from (5) for each well (Table 1); $\sigma[\ln(\phi_o)]$ is ±0.05 and $\sigma(1/D)$ is ±0.00005 m^{-1} from analysis of Western Platform data. The uncertainties (standard deviation) in $\Delta z'$ values (Table 1) range from ~±150 m in wells with relatively low $\Delta z'$ values to ~±850 m in wells with high $\Delta z'$ values and where the porosity data are more scattered (i.e., well Fresne-1; $\Delta z'$=2800 m). Apparent exhumation amounts

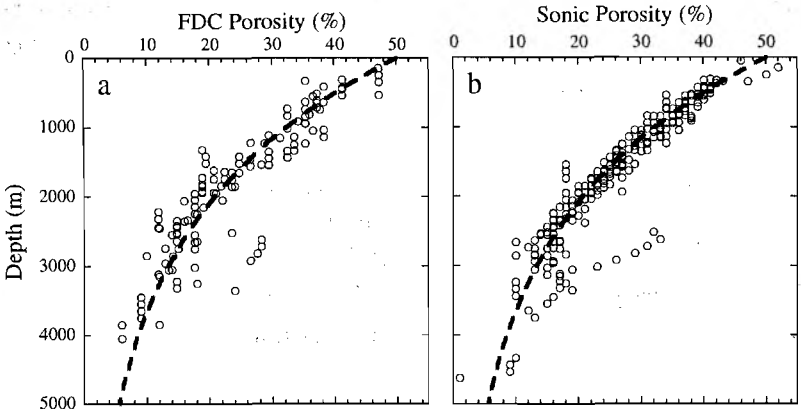

Figure 4. (a) Compensated formation density (FDC)-determined porosity and (b) sonic-determined porosity versus depth for Western Platform data. High values of porosity at depths of 2500-3500 m are caused by overpressure.

from porosity-depth trend offsets are combined with depths of known unconformities (see Table 1 and the appendix) to infer net exhumation amounts.

4. Eastern Mobile Belt Exhumation Patterns

The Eastern Mobile Belt region is divided for purposes of discussion into two regions: the southern region and the eastern region (Figure 7). These regions were chosen because they show large variations in exhumation amounts (Table 1) and have different geologic histories.

4.1. Exhumation in the Southern Region

The southern region includes the part of the Eastern Mobile Belt from wells south of and including the Maui-4–Moki-1-Kea-1 area (Figure 1) and is part of the Southern Inversion Zone of *King and Thrasher* [1996]. It is structurally dominated by east and west dipping, Miocene to Recent age thrust faults (Figures 1 and 2) that extend to the southwest from the Taranaki Basin proper to form a set of inverted basins in the west coast region of South Island [*Bishop and Buchanan*, 1995; *Kamp et al.*, 1996].

Maximum Neogene exhumation in Taranaki Basin occurred in the southern region of the Eastern Mobile Belt. Net exhumation amounts vary from about 220 ± 150 m in well Te Whatu-2 to a maximum of 3000 ± 860 m in Fresne-1. The average exhumation amount is 1350 m for the 11 southern region wells. Erosion was generally from the top of anticline structures that are associated with thrust faults (Figure 2) and as such should be thought of as local in nature. Erosion from discrete structures leads to large variations in exhumation amounts in short lateral distances. For example, exhumation decreases ~1000 m in the 10 km between Moki-1 and Kea-1 (Figures 1 and 7). Therefore exhumation contours across the structures are stylized and may not reflect actual exhumation amounts in the footwalls of thrusts.

The depth of the unconformity on which the apparent erosion occurred is ~200 m (Table 1 and Figure 2). The unconformity is overlain by Plio-Pleistocene age sediments and underlain, in well North Tasman-1, by New Zealand stage Tongapurutuan (~6-10 m.y.) age sediments. These ages suggest average erosion rates in the southern region were 325-650 m m.y.$^{-1}$ assuming that the time represented by the ages of the missing strata (ca. 4-8 m.y.) is evenly split between

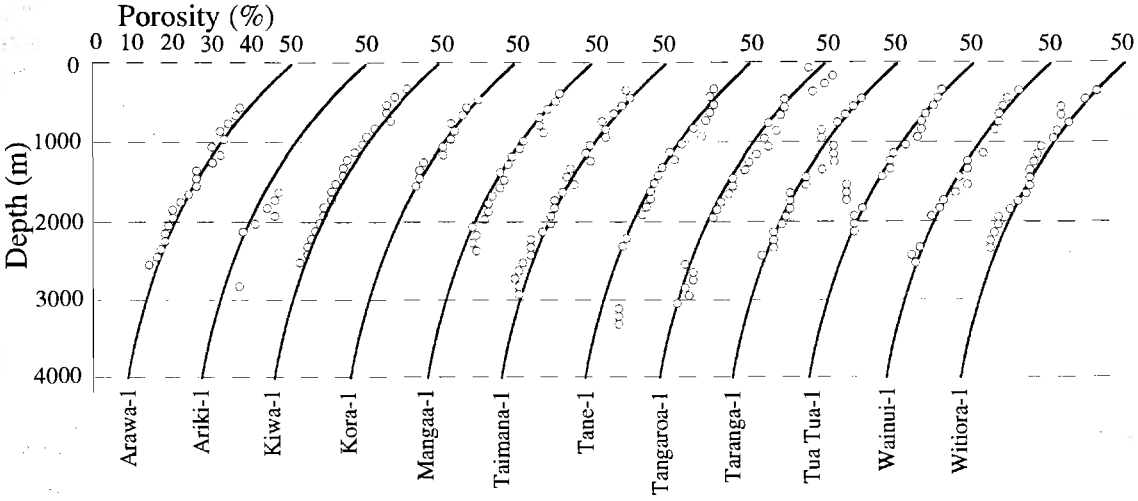

Figure 5. Composite plot of sonic-derived porosity versus depth for 12 Western Platform wells. The porosity scale is offset to show data for each well. The solid curve for each well is the standard porosity-depth curve for the Western Platform. Well names are listed at bottom of each curve; see Figure 1 for well locations.

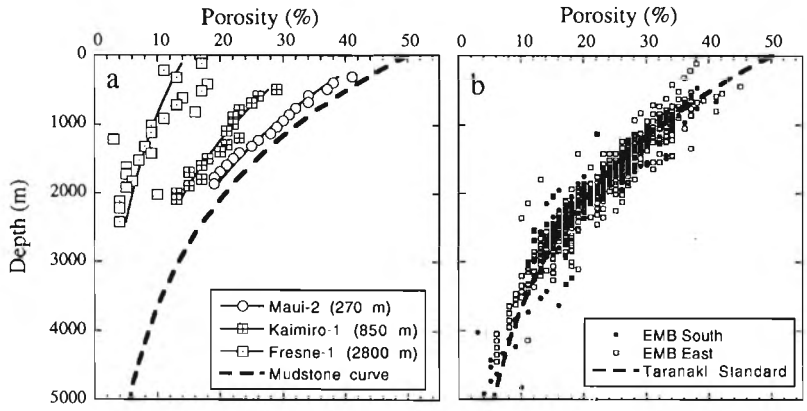

Figure 6. (a) Sonic-derived porosity versus depth for three representative wells from the Eastern Mobile Belt and (b) the porosity at corrected depths for all Eastern Mobile Belt wells. The dashed curve in both plots is the Western Platform standard porosity-depth curve. Numbers in parentheses in the legend of Figure 6a are average depth offsets of the porosity data from the standard curve for each well. Curves through the data are not best fit curves but are depth offset standard curves. Note the parallelism of the offset data trends to the standard curve. In Figure 6b, the depth-corrected data were corrected using the porosity-depth offset ($\Delta z'$ in Table 1) for each well.

deposition and erosion. On top of the growing structure at Fresne-1, erosion rates were ~700-1500 m m.y.$^{-1}$.

Other methods of exhumation estimation, such as seismic, fission track, and coal rank, also show that the southern Eastern Mobile Belt has undergone significant exhumation (Table 2). In general, the relative changes in exhumation estimates are similar between wells. The seismic reflection data, however, tend to give relatively high exhumation amounts relative to those determined in this study (Table 2). For example, well Cape Farewell-1 has an exhumation estimate of 1.5 km from offset porosity trends but >3 km from the seismic data. Exhumation estimates from seismic data are determined from vertical fault separation and from the vertical distance between the projection of apparently undisturbed units and tops of uplifted structures. Inherent in the estimate of erosion from the tops of structures as shown by seismic data is the assumption that relative uplift is equal to the exhumation amount. This may not be the case because uplift of rocks can occur without concomitant exhumation if the upper rock surface is subsea. Therefore the exhumation estimates determined from seismic data should be considered maximum amounts, and the true erosion amounts, at least in the southern Taranaki region, probably are represented better by offset porosity trends and by fission track and coal rank data because these data sets are keyed to an erosional datum that is at or above sea level.

4.2. Exhumation in the Eastern Region

The eastern region comprises the part of the Eastern Mobile Belt located east and north of the Maui-4–Moki-1-Kea-1 area (Figures 1 and 7). This region includes the following subregions, which are defined on the basis of fault patterns and styles after *King and Thrasher* [1996]: the Northern Graben, Southern Graben, Tarata Thrust Zone, and the northeast part of the Southern Inversion Zone.

Exhumation in the eastern region increases from the southwest to the northeast (Figure 7). In the southern part of this region, in a swath that extends southeast from the Maui Field to the Kupe/Toru/Tahi region (Figure 1), exhumation amounts are generally <400 m (Figure 7). To the northeast and on the Taranaki Peninsula, exhumation amounts steadily increase to a maximum of 1800 m at well Tatu-1 (Figure 7). Coal rank measurements [*Suggate*, 1959] from three wells (or coal fields adjacent to the well locations) imply a similar increase in exhumation from southwest to northeast across the Taranaki Peninsula. These estimates were determined by comparing coal rank values to the coal rank versus maximum depth of burial curve of *Sykes et al.* [1992] for Taranaki coals. In wells Toko-1, Puniwhakau-1, and Tatu-1, exhumation amounts from the offset porosity trends of this study are 640, 1360, and 1840 m, respectively (Figure 7), whereas corresponding coal rank-derived amounts are 400, 900, and 1800 m. Thus exhumation estimates from offset porosity trends and coal rank measurements show consistent trends.

The unconformity on which the apparent erosion recorded by the offset porosity trends occurred is either at the present erosional surface or buried 100-200 m by late Quaternary volcanic deposits from Mount Taranaki (Figure 2 and Table 1). The rocks under the unconformity are late Miocene-early Pliocene to the northeast and late Pliocene along the southern onshore region and offshore to the south. Therefore maximum age of erosion on the unconformity is late Pliocene in the southern areas and late Miocene to the northeast. It is likely, however, that the same erosional episode that began in the late Pliocene is responsible for exhuming the Miocene rocks and that any younger rocks that may have been present have since been removed by erosion. This scenario is supported by a continuous 2°-4° southwest tilt [*King and Thrasher*, 1996] of the middle Miocene to Pliocene strata on the onshore part of the basin, but it does not specifically exclude a component of late Miocene erosion that may have been associated with erosion in the southern region (see below).

Assuming a late Pliocene age (2 Ma) for the start of erosion, the average erosion rates have been 100-200 m m.y.$^{-1}$ for the southernmost onshore and offshore region, ~400 m m.y.$^{-1}$ for the middle of the Taranaki Peninsula, and ~900 m m.y.$^{-1}$ for the northeast area where exhumation has been greatest. Late Quaternary uplift rates based on uplifted marine terraces are ~250 m m.y.$^{-1}$ along the southern Taranaki Peninsula coast and increase to ~500 m m.y.$^{-1}$ toward the middle of the peninsula

Table 1. Eastern Mobile Belt Porosity Data

Well Name	Location[a]	Depth Fit Interval, mbsf	Well Depth, mbsf	Percent[b] Section, %	$\Delta z'$, m	Unconformity Depth, mbsf	Total Erosion, m	ϕ_0', %	Correlation Coefficient	n	$\sigma \ln(\phi_0')$[c] Well, %	$\sigma [\Delta z']$,[d] m
Cape Farewell-1	EMB South	91-1291	2808	43	1480	0	1480	26.0	-0.85	13	0.1	400
Cook-1	EMB South	442-1942	2529	59	730	100	830	36.2	-0.81	17	0.1	270
Fresne-1	EMB South	117-2417	2420	95	2800	200	3000	14.3	-0.78	23	0.3	860
Kea-1	EMB South	374-2074	3003	57	280	0	280	44.2	-0.97	18	0.1	220
Maui-4	EMB South	566-1966	3781	37	1020	300	1320	31.9	-0.92	15	0.1	300
Moki-1	EMB South	571-1971	2491	56	960	300	1260	32.8	-0.87	15	0.2	450
Motueka-1	EMB South	197-1397	1465	82	1280	200	1480	28.4	-0.89	13	0.1	370
N. Tasman-1	EMB South	382-1182	2614	31	1250	200	1450	28.8	-0.82	9	0.2	390
Surville-1	EMB South	540-1040	2140	23	1420	200	1620	26.7	-0.86	6	0.1	270
Te Whatu-2	EMB South	259-2259	3401	59	200	0	220	45.3	-0.96	31	0.1	150
Tasman-1	EMB South	191-1291	1521	72	1240	200	1440	29.0	-0.89	12	0.1	360
Awakino-1	EMB Eastern	538-1738	2838	42	1460	0	1460	26.2	-0.88	13	0.1	390
Cape Egmont-1	EMB Eastern	692-2392	2427	70	290	100	390	44.0	-0.95	18	0.1	270
Kaimiro-1	EMB Eastern	491-2091	4989	32	850	200	1050	34.4	-0.97	17	0.1	210
Kapuni Deep-1	EMB Eastern	391-1991	5651	28	240	100	340	45.0	-0.98	18	0.0	150
Kapuni-12	EMB Eastern	191-2891	3614	77	430	100	530	41.4	-0.87	28	0.1	220
Kapuni-9	EMB Eastern	1000-2100	3789	29	300	100	400	43.9	-0.94	12	0.1	190
Kiore-1	EMB Eastern	97-457	533	69	870	0	870	34.0	-0.78	5	0.0	190
Kupe South-4	EMB Eastern	532-3032	3784	66	160	0	160	46.5	-0.86	26	0.2	360
Kupe-1	EMB Eastern	61-2961	3643	80	-150	0	-150	53.5	-0.91	30	0.1	300
Manutahi-1	EMB Eastern	298-1348	1389	76	380	0	380	42.3	-0.95	13	0.0	140
Maui-1	EMB Eastern	682-3382	3392	80	170	0	170	46.3	-0.95	28	0.1	270
Maui-2	EMB Eastern	306-1861	3425	45	270	0	270	44.4	-0.99	18	0.0	140
Maui-6	EMB Eastern	159-2359	3087	71	280	0	280	44.1	-0.98	23	0.1	210
McKee-1	EMB Eastern	394-1694	3894	33	760	100	860	35.7	-0.96	14	0.1	190
Mokioa-1	EMB Eastern	692-1992	3742	35	140	0	140	47.0	-0.91	14	0.1	170
New Plymouth-2	EMB Eastern	295-2195	4447	40	770	100	870	35.7	-0.97	20	0.1	240
Okoki-1	EMB Eastern	568-3368	4176	43	1070	0	1070	31.2	-0.92	29	0.2	430
Onaero-1	EMB Eastern	294-2294	3584	56	820	0	820	34.8	-0.97	21	0.0	180
Pukearuhe-1	EMB Eastern	195-1295	3134	35	1340	0	1340	27.7	-0.86	12	0.1	400
Puniwhakau-1	EMB Eastern	95-1195	2141	51	1360	0	1360	27.4	-0.79	12	0.2	540
Stratford-1	EMB Eastern	190-2990	4965	56	620	200	820	38.1	-0.97	29	0.1	270
Tahi-1	EMB Eastern	289-1289	1665	60	370	0	370	42,4	-0.97	10	0.0	140
Tariki-1	EMB Eastern	393-2093	3181	53	850	0	850	34.4	-0.88	20	0.1	300

Table 1. (continued)

Well Name	Location[a]	Depth Fit Interval, mbsf	Well Depth, mbsf	Percent[b] Section, %	$\Delta z'$, m	Unconformity Depth, mbsf	Total Erosion, m	ϕ_0', %	Correlation Coefficient	n	$\sigma \ln(\phi_0')$[c] Well, %	$\sigma [\Delta z']$,[d] m
Tatu-1	EMB Eastern	97-797	857	82	1840	0	1840	22.2	-0.85	8	0.1	340
Te Kiri-1	EMB Eastern	593-2693	4703	45	350	100	450	42.9	-0.97	22	0.1	220
Te Ranga-1	EMB Eastern	223-923	3805	18	990	0	990	32.3	-0.58	8	0.2	400
Tipoka-1	EMB Eastern	492-2692	4351	51	300	100	400	43.7	-0.97	21	0.1	230
Toko-1	EMB Eastern	294-2894	4894	53	640	0	640	37.7	-0.98	27	0.1	220
Toru-1	EMB Eastern	468-2868	4103	58	50	0	50	48.8	-0.98	22	0.1	150
Turi-1	EMB Eastern	112-2912	4005	70	1220	0	1220	29.2	-0.90	29	0.2	510
Urenui-1	EMB Eastern	147-1977	3839	48	720	0	720	36.5	-0.91	21	0.1	260
Waihapa-1	EMB Eastern	394-1994	4471	36	440	0	440	41.1	-0.97	17	0.0	160

[a] EMB, Eastern Mobile Belt.
[b] Amount of mudstone-shale section used in analysis relative to amount penetrated by well.
[c] Standard deviation of $\ln(\phi_0')$ for n porosity-depth points for the well.
[d] Total standard deviation from (7).

[*Pillans*, 1986]. In addition, late Quaternary-Recent age faults have vertical slip rates of 100-400 m m.y.$^{-1}$ in the offshore region (Cape Egmont Fault Zone; [*Nodder* , 1993]) and 200 m m.y.$^{-1}$ onshore (Inglewood Fault [*Hull* , 1996]). Therefore late Pliocene to Recent erosion rates determined from offset porosity trends agree with the late Quaternary vertical uplift rates.

The late Miocene unconformity on which 1000-3000 m of exhumation occurred in the southern region is present at some of the southern well sites in the eastern region (wells of the Kapuni, Kupe, Tahi, and Manutahi areas in Figure 1), which are part of the Southern Inversion Zone of *King and Thrasher* [1996]. This unconformity is presently buried to depths of >1000 m under Plio-Pleistocene deposits across the southern part of the eastern region (Figure 7). Porosity-depth trends for wells in this area show that there are no apparent breaks in the porosity-depth trends, which indicates that the erosion on this unconformity was less than its present burial depth (<1000 m). Interpretation of seismic data [*King et al.*, 1991] suggests that the middle to late Miocene section is relatively thin on top of the Manaia Fault Zone (Figure 1) hanging wall structures and that growth of structures was below sea level and must have occurred during middle to late Miocene time [*King and Thrasher*, 1996]. Even though the vertical throw on the Manaia Fault is >2000 m in the vicinity of the Kapuni and Kupe structures (e.g., section B in Figure 2), the amount of relatively thin late Miocene section removed by erosion is only ~500 m. This erosion occurred late in the Manaia uplift history as the structure emerged above sea level and the erosional wave base. Farther north, Miocene rocks are at the surface or are unconformably overlain by Quaternary volcanic rocks, so that if the late Miocene unconformity did exist farther north, it has been removed by the late Pliocene erosional event. The decrease in exhumation on the late Miocene unconformity from the southern region (3000 m in Fresne-1) to the north (~500 m in Kapuni/Kupe area) suggests that any erosion on this unconformity even farther north onshore probably would have been small. Even though we cannot rule out Miocene erosion to the north and east on the peninsula, the lack of late Miocene structures similar to those of the Southern Inversion Zone [*King and Thrasher*, 1996] suggests that most of the exhumation observed in the northern well porosity-depth trends occurred on the late Pliocene unconformity.

5. Discussion

The exhumation patterns recorded by the offset porosity-depth trends (Figure 7) for the southern and eastern regions of the Taranaki Basin occurred at different times and were caused by different rock uplift mechanisms. They partially record spatial and temporal variations of rock uplift in this region adjacent to the Australian-Pacific plate boundary.

Late Neogene exhumation in the southern region is from the tops of inversion anticlines whereby older extensional basins were later exhumed by contractional tectonics. These structures extend farther south in the west coast region of South Island where coal rank data [*Suggate*, 1959], seismic interpretations [*Bishop and Buchanan*, 1995], and combined fission track, vitrinite reflectance, and thermal history

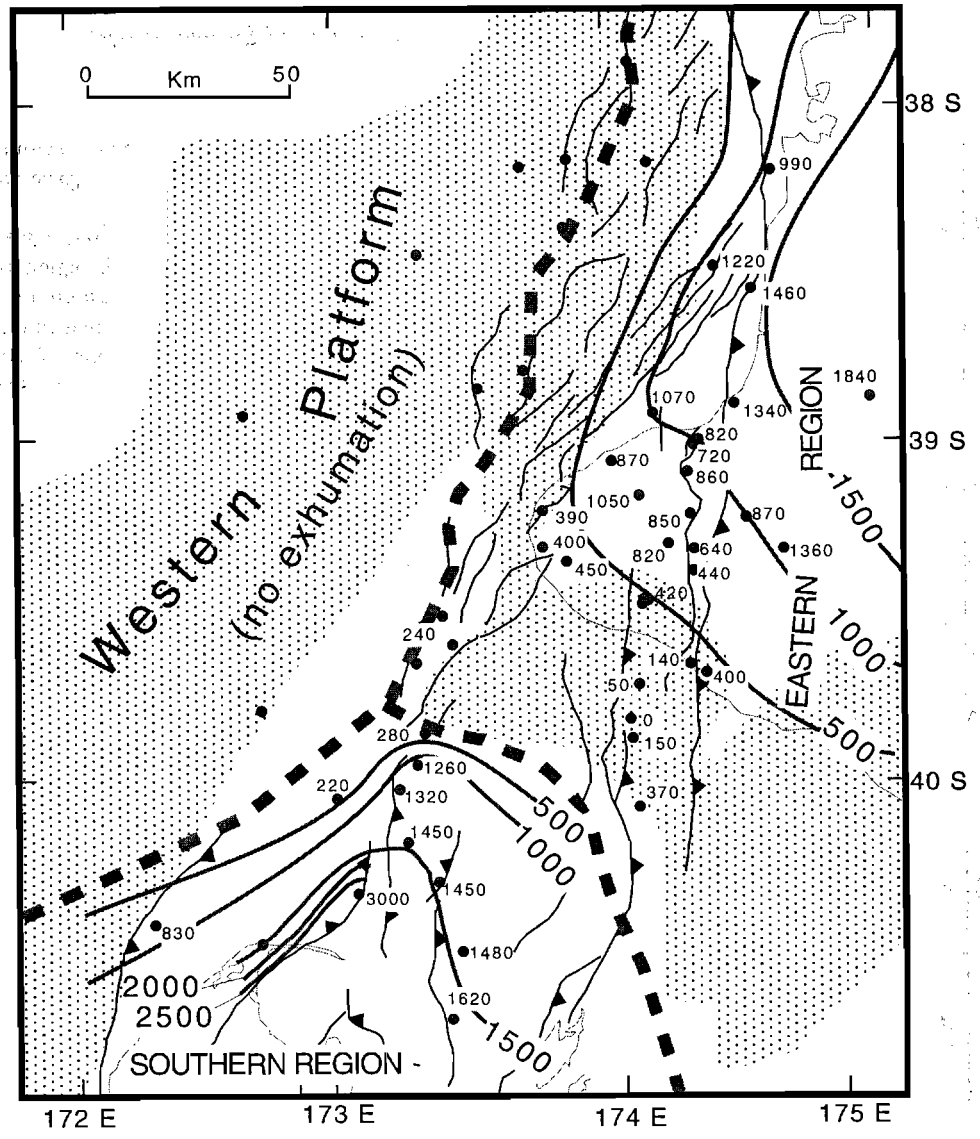

Figure 7. Net exhumation patterns in Taranaki Basin. Values are in meters and contours are in 500 m increments. Heavy dashed lines are boundaries between the Western Platform and the southern and eastern regions of the Eastern Mobile Belt. Stippled regions are areas where Plio-Pleistocene sediments are >1000 m thick [*Thrasher and Cahill*, 1990; *King and Thrasher*, 1996]. Exhumation amounts for the Kapuni, Kupe, and Maui fields are averages of the values in Table 1 for the wells in those fields.

analysis [*Kamp et al.*, 1996] indicate exhumation amounts of 2 km or more.

The southern region structural inversion and related rapid uplift and exhumation were probably caused by the reorganization of the southern end of the Hikurangi subduction zone presently located east of North Island of New Zealand and Taranaki Basin [*King and Thrasher*, 1996]. About 10 Ma a counterclockwise rotation of the Hikurangi subduction zone, associated with the southward migration of the Australia-Pacific pole of rotation [*Stock and Molnar*, 1982], caused renewed contraction across most of the southern Taranaki Basin and the west coast region. Also associated with this reorganization was accelerated convergence and rock uplift across the Alpine Fault to the southeast. Thus the area northeast of the Alpine Fault, as far north as the southern Taranaki Basin, and to the south and southeast along the Alpine fault was a broad region of horizontal contraction. In most of the southern Taranaki Basin this contraction caused localized uplift and erosion along discrete structures that lasted until ~5 Ma; however, the structure at the location of well Cook-1 (Figure 1) and those farther south onshore are still active [*King and Thrasher*, 1996].

Although the late Miocene-Pliocene exhumation documented in the southern region extends partly into the southern part of the eastern Taranaki region, almost all the exhumation recorded by the eastern region wells probably occurred since the Pliocene. The overall exhumation pattern progressively exposes Pleistocene rocks in the south to Miocene rocks farther north onshore, which is consistent with the regional 2°-4° southwest structural dip. The uniformity of the structural tilt and consistency of the exhumation pattern suggest that both were caused by the same rock uplift event.

Table 2. Southern EMB Erosion Estimate Comparisons

Well	Erosion Estimates, km			
	This Study	Seismic[a]	Fission[b] Track	Coal[c] Rank
Cape Farewell-1	1.5	>3.0	---	2.4
Cook-1	0.8	1.9	---	---
Fresne-1	3.0	>2.0-3.5	3.0	---
Kea-1	0.3	0.7	---	---
Moki-1	1.3	---	---	---
Motueka-1	1.3	2.0	---	---
N. Tasman-1	1.5	1.4	0.7-1.3	1.7-1.9
Surville-1	1.6	1.7-2.6	1.5-2.5	1.0
Maui-4	1.3	1.0-1.4	---	1.4-1.7
Tasman-1	1.4	2.0	---	---

[a] *Knox* [1982], *Ellyard and Beattie* [1990], and *King et al.* [1991].
[b] *Kamp and Green* [1990].
[c] *Sykes et al.* [1992].

The northeast increasing erosion pattern in Taranaki Basin is consistent with the erosion amounts based on coal rank data for most of western North Island (Figure 8). The broad and consistent exhumation pattern suggests that the erosional event was regional in nature, which contrasts with the more localized exhumation patterns in the southern Taranaki Basin.

Thermal uplift and flexural tilting are two mechanisms that can be invoked to explain the regional tilt and relative subsidence of the eastern Taranaki-South Wanganui basins. Exhumation increases toward the southern apex of the Central Volcanic Region on North Island (Figure 8). This region is a Pliocene-Recent age magmatic arc and associated rift basin characterized by thin crust, high heat flow, and crustal extension [*Stern*, 1987]. The coincidence of the trend of the Central Volcanic Region-South Wanganui Basin and the exhumation patterns (Figure 8) suggests that the tilt and subsequent erosion on western North Island may be associated with rift-flank and thermal uplift of the southern apex of the Central Volcanic Region. Even though thermal uplift can explain the regional exhumation patterns, it does not explain the overall subsidence that was occurring at the same time in the South Wanganui Basin where more than 3000 m of Plio-Pleistocene sediments were deposited. Deep seismic reflection and gravity data show that the South Wanganui Basin and eastern parts of the Taranaki Basin are underlain by thick (42 km) continental crust [*Stern and Davey*, 1990; *Holt and Stern*, 1994] that may be associated with late Tertiary subduction and crustal thickening [*Stern and Davey*, 1990]. In contrast to the thermal uplift interpretation, three-dimensional flexural modeling results suggest that the overall subsidence and tilting patterns in the South Wanganui Basin region can be explained by the slab pull force of the down going slab on the overriding plate [*Stern et al.*, 1992]. These models show crustal down warping in the region of South Wanganui Basin and synchronous uplift to the north and northeast. Although the exhumation patterns for the eastern Taranaki region of our study and the extrapolation farther north and northeast from coal rank data cannot differentiate between these two possible uplift mechanisms, they should place valuable constraints on further geodynamic modeling of this complex plate boundary region.

6. Conclusions

In this study we utilized a basin-wide comparison of compensated density and sonic travel time logs to develop a well-constrained transformation equation between travel time and porosity for Taranaki Basin mudstone/shale sequences. Travel time then can be used as a proxy for porosity where no other porosity information is available. In the Western Platform area, where no known exhumation has occurred, a best fit porosity-depth trend was developed from 12 wells over a depth range of 300-3000 m. This trend displays an exponential decrease in porosity with depth with an extrapolated surface porosity of 50% and an exponential decay constant of 2265 m.

Porosity-depth trends for the Eastern Mobile Belt are parallel to the Western Platform standard porosity-depth trend but are offset in depth from 0 to 2800 m. In the southern part of the Eastern Mobile Belt, net exhumation amounts (sum of offset porosity-depth trend and depth to erosional unconformity for each well site) range from 850 to 3000 m. This exhumation occurred in late Miocene to early Pliocene time in most of southern region well locations on discrete structures that formed when older basins were inverted to produce uplifted and eroded contractional structures. Contraction in this region of the Taranaki Basin was probably

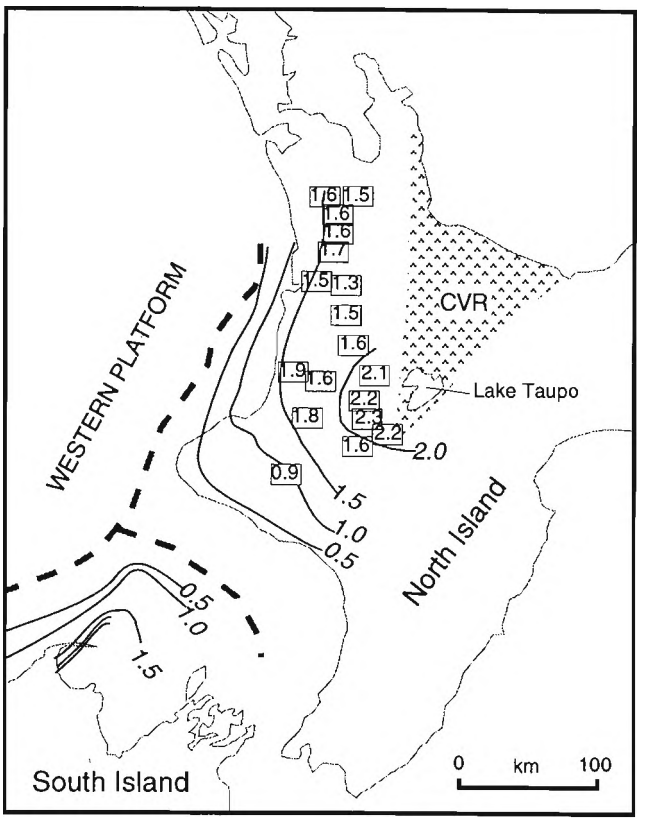

Figure 8. North Island map showing exhumation amounts from coal rank determinations. Exhumation amounts at each site are determined from the coal rank versus maximum depth of burial curve of *Sykes et al.* [1992] using the coal rank values from *Sykes et al.* [1992] and *Edbrooke et al.* [1994]. Contours are in 0.5 km increments and are the same as those in Figure 7, except for the 2.0 km contour derived from the coal rank data. CVR is Central Volcanic Region.

caused by counterclockwise rotation of the Hikurangi subduction zone and related increase in convergence rates along the Alpine Fault system located to the south and southeast.

In the eastern region of the Eastern Mobile Belt, net exhumation amounts increase from near zero along the southern onshore areas and just offshore to as much as 1800 m in the northeast part of the basin. This progressive northeast increase is consistent with a monoclinal 2°-4° SW tilt of Miocene to late Pliocene strata onshore. The regional and progressive pattern of exhumation in the eastern region is consistent with models of both thermal uplift and back arc flexural uplift patterns related to Plio-Pleistocene subduction zone plate interactions but contrasts with the discrete, structurally dominated exhumation patterns in the southern region.

Appendix: Generalized Exhumation and Burial Scenarios From Porosity Information

The apparent offset of porosity at various depths from the standard porosity-depth curve does not necessarily give the absolute amount of exhumation that may have occurred [*Magara*, 1978; *Hillis*, 1993]. Porosity offset is simply the sum of all periods of exhumation and burial at that location and is dependent on the number and depths of unconformities (paleo or present-day erosional surfaces). If the depths of unconformities are known, then the offset of porosity-depth trends can be used to infer absolute amounts of (or at least to place bounds on) exhumation and burial. Simply measuring offset of porosity trends and inferring exhumation amounts from them can lead to severe underestimates. In the following we describe generalized cases of burial/exhumation, where erosion is assumed to occur at sea level.

Varying periods of burial and erosion (Figure A1a) may lead to different porosity-depth trends (Figures A1b-A1f). The resulting porosity-depth curve at t_1 is not displaced from the normal porosity-depth curve (Figure A1b) because there has not yet been a period of erosion. It is wells like these, such as those on the Western Platform, with no periods of erosion that are used to derive the standard porosity-depth curve.

At t_2 in the burial history the rock column has experienced an amount of exhumation E equal to the amount of porosity-depth curve offset ($\Delta z'$ in Figure A1b) with an unconformity depth (z_{un}) of zero. If z_{un} is not zero (Figure A1c and time t_4 in Figure A1a) and if the depth range of the fitting function used to determine the displacement of porosity-depth data from the standard porosity-depth curve is below the unconformity, then the net exhumation amount is not the porosity-depth offset but is the sum of the offset and the depth of the unconformity below sea level:

$$E = \Delta z' + z_{un}. \qquad \text{(A1)}$$

Well Maui-4 in the southern part of Taranaki Basin (Figure 1) is an example of this scenario.

At time t_5, z_{un} is greater than the previous erosion amount, and the porosity-depth curve falls back onto the standard curve upon which it would continue down with further burial. In this case, only a maximum bound can be placed on the exhumation amount, namely, exhumation E is less than or equal to the depth of the unconformity. This composite exhumation/burial scenario could lead to the erroneous interpretation of zero exhumation when in fact there may have been substantial erosion prior to the most recent burial. Kupe Field wells in the southeastern part of Taranaki Basin (Figure 1) are examples of this scenario.

It is common that a borehole encounter more than one unconformity, each of which may contribute to the net offset

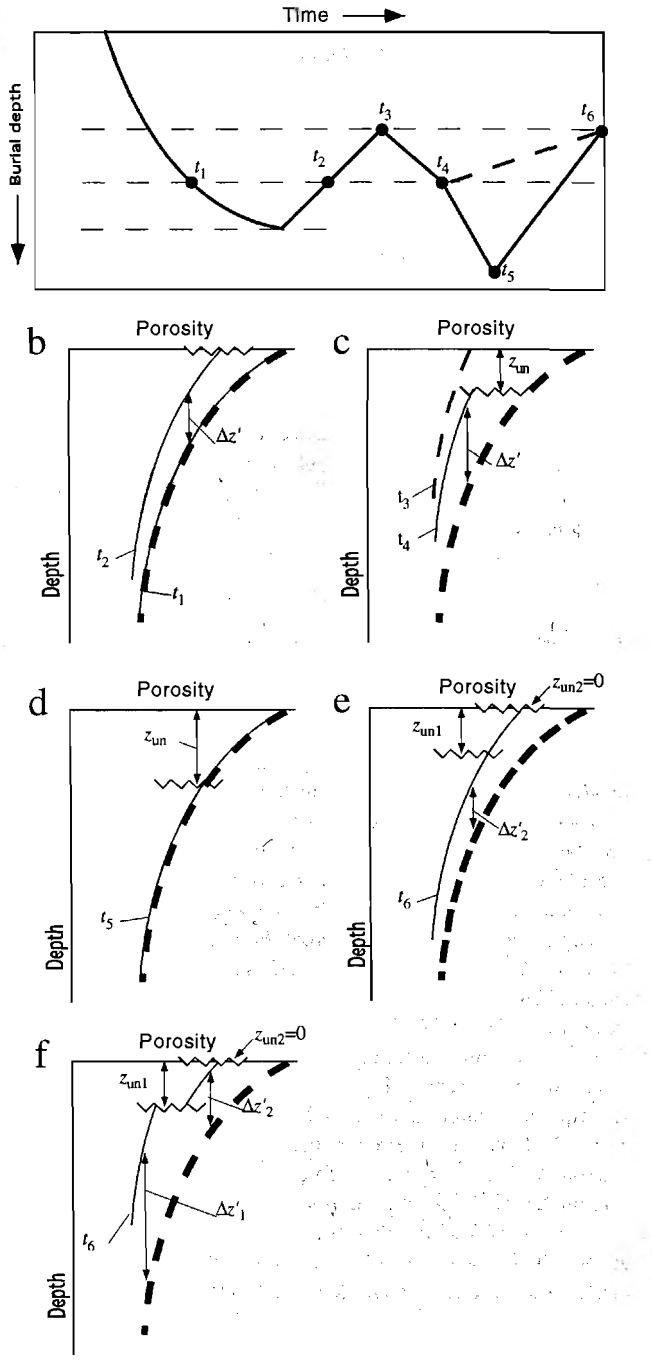

Figure A1. (a) Schematic burial/erosion versus time and (b)-(f) porosity versus depth trends to illustrate porosity-depth trends for different example burial/exhumation histories. In all plots the t values represent different times in the history, $\Delta z'$ is the offset amount of porosity-depth trends, and z_{un} refers to depths of unconformities. In Figures A1b-A1f, the bold dashed curve is the standard porosity-depth trend and the solid curves represent offset porosity-depth trends. Horizontal zig-zags are unconformities. See text for discussion.

of the porosity-depth curve. The actual amount of exhumation recorded by the porosity offset for a particular unconformity or set of unconformities depends on the depth range of the fitting function relative to the depth of the unconformities. If the depth range is between two unconformities, then the offset of the porosity-depth curve is related only to erosion on the upper unconformity. If the depth range is below the lowest unconformity, then the porosity-depth offset is related to the combined erosion on the two unconformities. If the depth range is solely above the top unconformity, then the porosity-depth offset contains no information about erosion on the unconformities. Ideally, the depth range should be chosen to lie between known unconformities in order to distinguish exhumation amounts on each.

Figure A1e illustrates the porosity-depth offset and unconformity depth relations for two periods of exhumation with a burial event in between at time t_5 that is greater than the previous maximum burial. At time t_6 the depth to the upper unconformity (z_{un2}) is zero and the exhumation amount (E_2) on the upper unconformity is equal to the offset on the porosity-depth curve ($\Delta z'_2$ in Figure A1e). If further burial occurs, then the exhumation amount is computed as the sum of offset porosity-depth curve and depth of unconformity, as in (A1) above. Since the maximum burial amount at time t_5 was greater than the previous burial amount, there is no break in the porosity-depth curve at the lower unconformity, and the exhumation amount on the lower unconformity is less than the second burial amount plus the porosity-depth trend offset ($E_1 < z_{un1} + \Delta z'_2$). However, if the maximum burial during the second burial period (time t_4) was less than during the first burial period with uplift and exhumation shown by a dashed line between times t_4 and t_6, then a break in the porosity-depth curve will occur at the deeper unconformity and the exhumation amount there will be $E_1 = \Delta z'_1 + z_{un1} + E_2$, where $\Delta z'_1$ is the offset of the porosity-depth curve below the lower unconformity (Figure A1f).

In summary, though porosity-depth offset gives apparent exhumation amounts, each must be evaluated in terms of the numbers and depths of known unconformities as well as the depth range of the porosity data used to determine the porosity-depth offset. In many cases, such as where older unconformities are eroded through or where burial is greater than previous exhumation amounts, only limits can be placed on the actual net exhumation amount. In these special cases, other geologic evidence is required to refine the net exhumation amount.

Acknowledgments. Armstrong and Chapman acknowledge the donors of The Petroleum Research Fund, administered by the American Chemical Society, for support of this research. Allis and Funnell acknowledge the support of the Petroleum Resources of New Zealand research program funded by the N.Z. Foundation for Research, Science, and Technology. R. Jarrard and M. Perkins reviewed an earlier version of this paper. We are grateful to M. Perkins for help with the statistics and to P. King and G. Thrasher for clarifying the tectonics of the Taranaki region. P. Knuepfer, an anonymous reviewer, and Associate Editor D. Merritts provided careful and insightful reviews.

References

Athy, L.F., Density, porosity and compaction of sedimentary rocks, *AAPG Bull.*, *14*, 1-24, 1930.

Baldwin, B., and C.O. Butler, Compaction curves, *AAPG Bull.*, *69*, 622-626, 1985.

Bishop, D.J., and P.G. Buchanan, Development of structurally inverted basins: A case study from the West Coast, South Island, New Zealand, in *Basin Inversion*, edited by J.G. Buchanan and P.G. Buchanan, *Geol. Soc. Spec. Publ.*, *88*, 549-585, 1995.

Davis, E.E., and H. Villinger, Tectonic and thermal structure of the Middle Valley sedimented rift, northern Juan de Fuca Ridge, *Ocean Drill. Program Proc. Initial Rep.*, *139*, 9-41, 1992.

Edbrooke, S.W., R. Sykes, and D.T. Pocknall, *Geology of the Waikato Coal Measures, Waikato Coal Region, New Zealand*, Inst. of Geol. and Nucl. Sci., Lower Hutt, New Zealand, 1994.

Ellyard, T., and B. Beattie, Inversion structures and hydrocarbon potential of the Southern Taranaki Basin, paper presented at *1989 New Zealand Oil Exploration Conference*, Minist. of Comm., Wellington, N.Z., 1990.

England, P., and P. Molnar, Surface uplift, uplift of rocks, and exhumation of rocks, *Geology*, *18*, 1173-1177, 1990.

Falvey, D.A., and I. Deighton, Recent advances in burial and thermal geohistory analysis, *APEA J.*, *22*, 65-81, 1982.

Gallagher, K., An examination of some uncertainties associated with estimates of sedimentation rates and tectonic subsidence, *Basin Res.*, *2*, 97-114, 1989.

Hamilton, E.L., Variations of density and porosity with depth in deep-sea sediments, *J. Sediment. Pet.*, *46*, 280-300, 1976.

Hayward, B.W., and R.A. Wood, Computer-generated plots for Taranaki drill hole sequences, *Rep. N.Z. Geol. Surv., PAL 147*, 1-73, 1989.

Heasler, H.P., and N.A. Kharitonova, Analysis of sonic well logs applied to erosion estimates in the Bighorn Basin, Wyoming, *AAPG Bull.*, *80*, 630-646, 1996.

Hillis, R.R., Quantifying erosion in sedimentary basins from sonic velocities in shales and sandstones, *Explor. Geophys.*, *24*, 561-566, 1993.

Holt, W.E., and T.A. Stern, Subduction, platform subsidence, and foreland thrust loading: The late Tertiary development of Taranaki Basin, New Zealand, *Tectonics*, *13*, 1068-1092, 1994.

Hull, A.G., Earthquake and volcanic hazards in Taranaki: Potential threats to oil and gas production and distribution infrastructure, paper presented at 1996 New Zealand Petroleum Conference Proceedings, Minist. of Comm., Wellington, N.Z., 1996.

Issler, D.R., A new approach to shale compaction and stratigraphic restoration, Beaufort-Mackenzie basin and Mackenzie Corridor, northern Canada, *AAPG Bull.*, *76*, 1170-1189, 1992.

Kamp, P.J., and P.F. Green, Thermal and tectonic history of selected Taranaki Basin (New Zealand) wells assessed by apatite fission track analysis, *AAPG Bull.*, *74*, 1401-1419, 1990.

Kamp, P.J.J., K.S. Webster, and S. Nathan, Thermal history analysis by integrated modelling of apatite fission track and vitrinite reflectance data: Application to an inverted basin (Buller Coalfield, New Zealand), *Basin Res.*, *8*, 383-402, 1996.

King, P.R., The habitat of oil and gas in the Taranaki basin, paper presented at 1994 New Zealand Oil Exploration Conference, Minist. of Comm., Wellington, N.Z., 1994.

King, P.R., and G.P. Thrasher, Post-Eocene development of the Taranaki Basin, New Zealand: Convergent overprint of a passive margin, in *Geology and Geophysics of Continental Margins*, edited by J.S. Watkins, F. Zhiqiang, and K.J. McMillen, *AAPG Memoir*, *53*, 93-118, 1992.

King, P.R., and G.P. Thrasher, *Cretaceous-Cenozoic geology and Petroleum Systems of the Taranaki Basin, New Zealand*, 243 pp., 6 enclosures pp., Inst. of Geol. and Nucl. Sci., Lower Hutt, N.Z., 1996.

King, P.R., T.R. Naish, and G.P. Thrasher, Structural cross sections and selected palinspastic reconstructions of the Taranaki basin, New Zealand, *Rep. N.Z. Geol. Surv., G150*, 7 sheets, 1991.

Knox, G.J., Taranaki Basin, structural style and tectonic setting, *N.Z. J. Geol. Geophys.*, *25*, 125-140, 1982.

Korvin, G., Shale compaction and statistical physics, *Geophys. J. R. Astron. Soc.*, *28*, 35-50, 1984.

Magara, K., Thickness of removed sedimentary rocks, paleopore pressure, and paleotemperature, southwestern part of western Canada basin, *AAPG Bull.*, *60*, 554-566, 1976.

Magara, K., *Compaction and Fluid Migration: Practical Petroleum Geology*, 319 pp., Elsevier Sci., New York, 1978.

Mood, A.M., F.A. Graybill, and D.C. Boes, *Introduction to the Theory of Statistics*, 564 pp., McGraw-Hill, New York, 1974.

Nodder, S.D., Neotectonics of the offshore Cape Egmont Fault Zone, Taranaki Basin, New Zealand, *N.Z. J. Geol. Geophys.*, *36*, 167-184, 1993.

Pilaar, W.F.H., and L.L. Wakefield, Structural and stratigraphic evolution of the Taranaki Basin, offshore North Island, New Zealand, *APPEA J.*, *18*, 93-101, 1978.

Pillans, B., A late Quaternary uplift map for North Island, New Zealand, in *Recent Crustal Movements of the Pacific Region*, edited by W.I. Reilly and B.E. Harford, *Bull. R. Soc. N.Z.*, *24*, 409-417, 1986.

Press, W.H., S.A. Teukolsky, W.T. Vetterling, and B.P. Flannery, *Numerical Recipes*, 963 pp., Cambridge Univ. Press, New York, 1992.

Sclater, J.G., and P.A.F. Christie, Continental stretching: An explanation of the post-mid-Cretaceous subsidence of the central North Sea Basin, *J. Geophys. Res.*, *85*, 3711-3739, 1980.

Selley, R.C., Porosity gradients in the North Sea oil-bearing sandstones, *J. Geol. Soc. London*, *135*, 119-132, 1978.

Stern, T.A., Asymmetric back-arc spreading, heat flux, and structure associated with the Central Volcanic Region of New Zealand, *Earth Planet. Sci. Lett.*, *85*, 265-276, 1987.

Stern, T.A., and F.J. Davey, Deep seismic expression of a foreland basin: Taranaki basin, New Zealand, *Geology*, *18*, 979-982, 1990.

Stern, T.M., G.M. Quinlan, and W.E. Holt, Basin formation behind an active subduction zone: Three dimensional flexural modelling of Wanganui basin, New Zealand, *Basin Res.*, *4*, 197-214, 1992.

Stock, J., and P. Molnar, Uncertainties in relative positions of the Australia, Antarctica, Lord Howe, and Pacific plates since the Late Cretaceous, *J. Geophys. Res.*, *87*, 4697-4714, 1982.

Suggate, R.P., New Zealand coals, *DSIR. Bull. N.Z.*, *134*, 1-113, 1959.

Sykes, R., R.P. Suggate, and P.R. King, Timing and depth of maturation in southern Taranaki Basin from reflectance and Rank(S), paper presented at 1991 New Zealand Oil Exploration Conference, Minist. of Comm., Wellington, N.Z., 1992.

Thrasher, G.P., and J.P. Cahill, Subsurface maps of the Taranaki Basin, New Zealand, *Rep. N.Z. Geol. Suv.*, *G142*, 45 pp., 14 sheets, 1990.

Wells, P.E., Porosities and seismic velocities of mudstones from Wairarapa and oil wells of North Island, New Zealand, and their use in determining burial history, *N.Z. J. Geol. Geophys.*, *33*, 29-39, 1990.

Wyllie, M.R.J., A.R. Gregory, and L.W. Gardner, An experimental investigation of factors affecting elastic wave velocities in porous media, *Geophysics*, *25*, 459-493, 1956.

R. G. Allis, Energy and Geoscience Institute, University of Utah Research Park, 423 Wakara Way, Salt Lake City, UT 84108-1210.

P. A. Armstrong and D. S. Chapman, Department of Geology and Geophysics, University of Utah, Salt Lake City, UT 84112-7065. (e-mail: paarmstr@mines.utah.edu)

R. H. Funnell, Institute of Geological and Nuclear Sciences, Lower Hutt, New Zealand.

(Received November 3, 1997; revised June 9, 1998;
accepted August 25, 1998.)